ISTITUTO NAZIONALE DI FISICA NUCLEARE

Sezione di Milano

INFN/TC-93/01
26 Marzo 1993

F. Broggi, S. Piuri, L. Rossi:

AN APPARATUS FOR THERMAL CONDUCTIVITY MEASUREMENTS AT CRYOGENIC TEMPERATURE ON COIL BLOCKS

PACS.: 07.20.Mc

Servizio Documentazione
dei Laboratori Nazionali di Frascati

INFN – Istituto Nazionale di Fisica Nucleare
Sezione di Milano

INFN/TC–93/01
26 Marzo 1993

AN APPARATUS FOR THERMAL CONDUCTIVITY MEASUREMENTS AT CRYOGENIC TEMPERATURE ON COIL BLOCKS

F. Broggi, S. Piuri, L. Rossi

INFN – Sezione di Milano e Dipartimento di Fisica dell'Universita' di Milano, Laboratorio LASA, Via Fratelli Cervi 201, 20090 Segrate

ABSTRACT

The effective thermal conductivity in the transverse direction is one of the less predictable parameters of a superconducting coil. In the framework of the construction of a high field solenoid (18 Tesla – 100 mm free bore at 4.2 K) at the LASA lab, we built an apparatus for measurements of thermal conductivity of pure materials as well as of composites and coil blocks, the main aim of the experiment being the measurements of the thermal conductance of pieces of real NbTi and Nb_3Sn windings. This paper starts with a discussion of how the thermal conductivity affects quench properties of superconducting magnets. The main features of the experimental apparatus are described together with a calculation and a measurement of the thermal loss. Finally preliminary measurements on some pure materials as well as on coil blocks are presented.

1 INTRODUCTION

Magnetic fields in the range 10 to 20 Tesla by means of superconducting magnets are nowadays available. Nevertheless the problems of reliable operation and of protection in case of quench is still open and under investigation. This is especially true when very high fields, B $\geq$ 15 Tesla, are reached by means of superconducting coupled adiabatic coils[1][2] [3]. In fact the use of fully epoxy impregnated coils wound with cable with small amounts of copper (or without) is very effective in cost saving but can result in poor protection of the magnet in case of quench and several papers have been recently published about the quench propagation[4][5]. In our lab we are developing a numerical code to describe the quench propagation in adiabatic, multicoil, multisection magnets[6].

It has been shown[4][5] that in an adiabatic magnet the transverse propagation, i.e. turn to turn and layer to layer, is the dominant mechanism of the quench propagation. While the longitudinal propagation, along the cable, is dominated by heat diffusion through the metal, the transverse one is mainly determined by the heat diffusion through the insulation.

The longitudinal velocity of the normal zone propagation, v_l, can be analytically derived and the transverse velocity v_t is usually given as :

$$v_t = v_l \times \sqrt{\lambda_t / \lambda_l}$$

where λ_l and λ_t are the longitudinal and transverse thermal conductivities of the winding. This simple expression can be modified, according to[7], to take into account the fact that heat does not diffuse significantly into the resin in the longitudinal propagation but it does so in the transverse one. The importance of the effective thermal conductivity of the winding is evident in the above formula.

The values of λ_l can be fairly well calculated, both as a function of temperature and magnetic field. Indeed it involves only properties of metals, mainly of the copper. Even in the case of a small percentage of copper, or no copper at all, λ_l can be calculated with a reasonable degree of accuracy by considering all the metals of the cable acting as thermal conductances in parallel.

Very different considerations apply to the evaluation of λ_t. Wires for high field are generally composed of Nb_3Sn or $(NbTa)_3Sn$ filaments embedded in a CuSn matrix and generally the stabilizing copper is protected by a thin barrier made out of tantalum or other suitable materials and a simple model based on parallel or series of thermal conductances is not reliable. The situation is more complicated for multistrand cables, where the interstrand contacts can give a non negligible contribution to the transverse heat conduction, even if the twist of the cable can reduce the importance of the interstrand thermal contacts.

Even if λ along the cross section of the cable can be computed, one must still evaluate λ through the insulation, the most relevant parameter. The insulation is generally either glass braid (or tape) or, for NbTi single wire, a thin coating of enamel (such as formvar). After casting of the coil with epoxy resin, in the case of glass insulation one has a composite whose properties can be thought very similar to the properties of G10 or G11 fiber glass composite. In case of formvar insulation generally the thermal properties of formvar-epoxy composite are considered to be similar to the epoxy resin.

The thermal conductivity of the resin- glass fibre composite is not so easy to predict as it is for the metals and different values are given in the literature[8][9] and in the case of a composite like epoxy - glass braid the relative cross section of every component is difficult to determine and depends on the considered directions (anisotropy). Moreover, another

source of uncertainty is given by the effective thermal transmission between the metal and the insulation, i.e. the surface conditions can strongly affect the quality of bonding between the different elements, with possible non negligible surface thermal resistance.

While different approximations in computing the effective λ_t of the winding can give a reasonable degree of accuracy, we believe that an effort to work out the above described problems can be useful in reaching a better prediction of the normal zone growth in adiabatic superconducting magnets. In particular it should be very useful to have data both of any single component and of the composite, versus temperature and at different magnetic field levels, especially in the 20 Tesla range.

We started an experimental program aiming to build two thermal conductimeters. One is for measurements of λ of rods or bars and will be used for metals, cables, insulators. The other conductimeter will be mainly dedicated to measurements on coil blocks, cut out from real windings, and on composite materials which are difficult to obtain in bar. In this conductimeter it is possible to measure samples under low or moderate pressure. Both the systems can work between 2 and 350 K. In 1994, when the high field facility *SOLEMI* [1] will be at our disposal, the two thermal conductimeters will be arranged to perform measurements of $\lambda = \lambda(T, B)$.

2 THEORY OF MEASUREMENT

The thermal conductivity represents the capability of a material to transport heat between two side at different temperature, without net mass flow.

Macroscopically, it is defined as the heat (in a time unit) which flows in a steady state through a plate with section S, thickness L and thermal gradient ΔT between sides:

$$\dot{Q} \propto S\frac{\Delta T}{L} \tag{1}$$

Generalizing, this relation can represent the Fourier - Biot law:

$$\dot{Q} = -\lambda\, S\, \frac{dT}{dl} \tag{2}$$

where λ is the thermal conductivity and it generally is a function of T. The negative sign means that the power flows in direction opposite to the thermal gradient.

There are many different techniques to measure λ, which can span more than 5 order of magnitude passing from an insulator to a metal. We can distinguish between stationary methods (called static) and non stationary ones (dynamic); in the first one, a time constant thermal gradient is produced into the sample and once a steady state is reached, the thermal conductivity is directly obtained by measuring the heat flow per unit area and the thermal gradient.

Heat flow then can be radially or axially directed: in the first case a cylindric or spheric sample is crossed by a radial heat flow directed from the axis (cylinder) or the center (sphere) to the center surface. In the second case, a cylinder is crossed by a longitudinal (along the axis) heat flow. In any case all possible technical solutions are used in order to reduce radiative and convective thermal losses.

Using the experimental method of the axial heat flow the thermal conductivity, can be obtained by (derivative approximated method):

$$\lambda = -\frac{\dot{Q} L}{S\ \Delta T} \tag{3}$$

which comes from:

$$\lambda(T) = -\frac{\dot{Q}}{S}\frac{dl}{dT} \tag{4}$$

replacing dl/dT with $L/\Delta T$ and considering S as a constant. The integration of the equation 4 between T_1 and T_2 gives:

$$\int_{T_1}^{T_2} \lambda(T)\ dT = \int_{T_1}^{T_2} -\frac{\dot{Q}}{S}\frac{dl}{dT}\ dT = -\frac{\dot{Q}}{S}\ L \tag{5}$$

showing that the equation 3 represents the mean value of $\lambda(T)$ in the temperature range between T_1 and T_2:

$$\bar{\lambda}(T_1, T_2) = \frac{1}{\Delta T}\int_{T_1}^{T_2} \lambda(T)dT = -\frac{\dot{Q}L}{S\ \Delta T} \tag{6}$$

According to this method we assign this λ "mean value" to the mean temperature between T_1 and T_2, that means:

$$\lambda(\bar{T}) \equiv \bar{\lambda} \tag{7}$$

where:

$$\bar{T} = \frac{T_1 + T_2}{2} \tag{8}$$

Actually $\lambda(\bar{T}) = \bar{\lambda}$ only if $\lambda(T)$ is a linear function of T, or a constant one, otherwise this approximation holds only if ΔT is small. But even if ΔT is few tens of degrees the error is always very small if $\lambda(T)$ is a slowly varying function of the temperature [10]. For example, in figure 10 is shown a comparison between measured and tabulated tungsten thermal conductivity: the values of λ at temperature of 20 K or next to it are derived with temperature differences of about $20 \div 30$ K. Here λ is not a locally rapidly varying function of T and, as it can be seen, the errors are very small. A useful quantity, that will be used later, is the thermal conductance, defined from the Fourier - Biot law as

$$\dot{Q} = C\Delta T \qquad so \qquad C = \frac{\dot{Q}}{\Delta T} = \bar{\lambda}(T_1, T_2)\frac{S}{L} \tag{9}$$

Our interest is mainly directed to the measurements of composite materials, like superconductive wires or coil blocks. The previous equations can be used to obtain a simple theoretical model describing these situations.

In fact, in case of a composite material, where the thermal conductivity of each component is known, a theoretical evaluation of the effective conductivity can be done, describing the composite by an appropriate model. As a matter of fact, a coil block can be represented as a sequence of different materials thermically connected in series and, from the Fourier - Biot law, we get

$$\lambda_{eff}(\bar{T}) = -\frac{\dot{Q}}{S}\frac{L}{\Delta T} \tag{10}$$

In this case the above relation cannot be directly integrated, without knowing the temperature profile along the sample. Once the temperature profile is known, the integration of the thermal conductivity can be done and the value of the conductance and of the mean conductivity can be determined.

Neglecting radiative and convective losses the temperature profile is determined by the continuity condition

$$\frac{d\dot{Q}}{dx} = 0 \tag{11}$$

That is

$$\frac{d}{dx}(\lambda(T)S(x)\frac{dT}{dx}) = 0 \tag{12}$$

That drives to the equation

$$\frac{d^2T}{dx^2} + \frac{1}{\lambda(T)}\frac{d\lambda(T)}{dT}(\frac{dT}{dx})^2 + \frac{1}{S(x)}\frac{dS(x)}{dx}\frac{dT}{dx} = 0 \tag{13}$$

With the boundary conditions

$$T(x=0) = T_1 \qquad T(x=L) = T_2 \tag{14}$$

The solution of the equation cannot be analytically determined, being non linear and with variable coefficients; furthermore there is no analytical relation for the values of $\lambda(T)$, that are determined by a linear interpolation of experimental data. Therefore a numerical code has been developed in order to solve the equation 13 and to compare the "theoretical data" for λ_{eff} for a composite material (where the $\lambda(T)$ of each component is known) and the measured λ_{eff}.

To solve the equation, the Taylor method with the procedure of the "garden hose" has been used. The method of Taylor consists in dividing the length of the conductor into equal segments and propagating the solution using the Taylor expansion, thus:

$$T(x+\Delta x) \simeq T(x) + (\frac{dT}{dx})\mid_x \Delta x + \frac{1}{2}(\frac{d^2T}{dx^2})\mid_x (\Delta x)^2 \tag{15}$$

The second derivative is given by 13. The second order expansion gives good approximation of the solution so we did not tried to use higher order.

At the first step we guess a possible value of $(dT/dx)\mid_0$. The first derivative at the following steps is calculated by the continuity condition, 11, $dotQ(x) = dotQ(x+\Delta x)$:

$$\lambda(T)S(x)(\frac{dT}{dx})\mid_x = \lambda(T(x+\Delta x))S(x+\Delta x)(\frac{dT}{dx})\mid_{x+\Delta x} \tag{16}$$

$$(\frac{dT}{dx})\mid_{x+\Delta x} = \frac{\lambda(T)S(x)(\frac{dT}{dx})\mid_x}{\lambda(T+\Delta T)S(x+\Delta x)} \tag{17}$$

Starting from the lower terminal, $x = 0$, step by step the temperature $T(L)$ of the higher terminal is calculated. Then the initial slope guess is modified until the calculated temperature profile satisfies the upper boundary condition T(L) = T_2 (garden hose procedure).

This model can describes only a sequence of materials, it is clear that the model is quite simple, because a superconducting coil has a quite complex composition; furthermore no thermal resistance at the interfaces between the materials is taken into account.

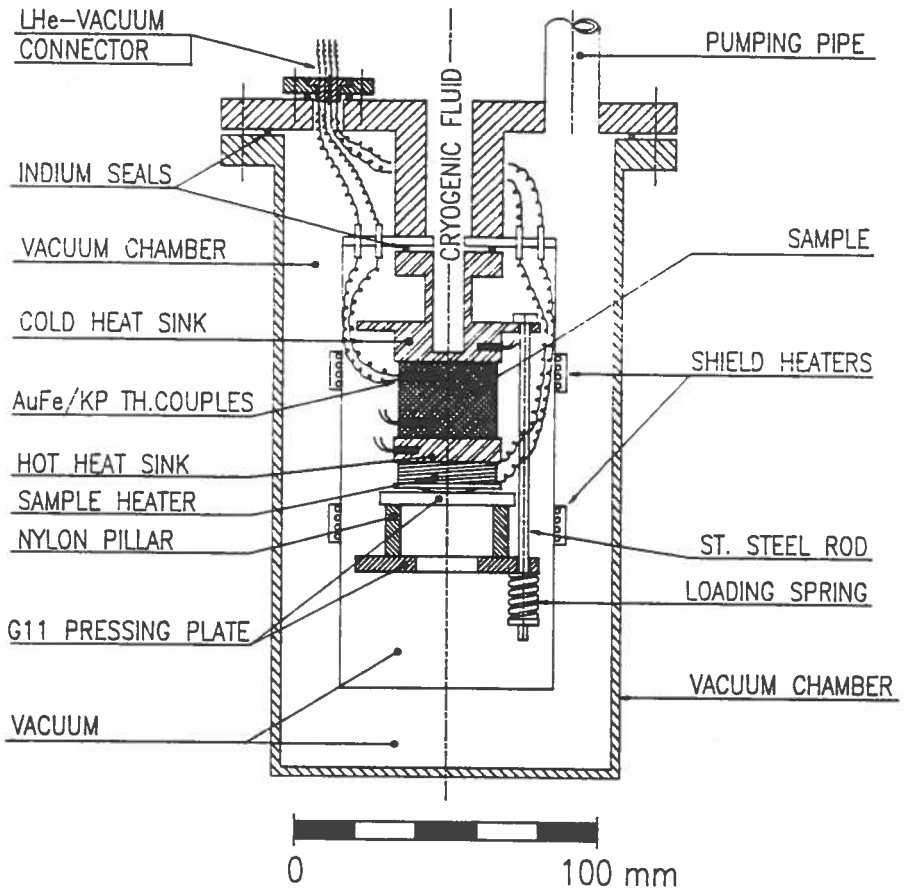

Figure 1: Sketch of the thermal conductimeter

3 DESCRIPTION OF THE MEASUREMENT APPARATUS

The apparatus has been designed in order to measure the transverse thermal conductivity with the stationary method of the axial heat flux. The apparatus is basically constituted by 2 heat sinks at different temperatures; the sample is placed between them. The cold heat sink is at direct contact with the cryogenic fluid, while the warm one is typically an electric heater [11]. Two or more temperature sensors are placed along the sample, and, in stationary conditions, knowing the power flowing through the sample, the value of the thermal conductivity can be determined through the Fourier - Biot law.

$$\lambda(\bar{T}) \simeq \frac{\dot{Q} L}{S \, \Delta T} \tag{18}$$

In fig. 1 a section of the measurement apparatus is shown. The block of the material under measurement (the sample) is held between the copper heat sinks by a pressing system, in order to have a good thermal contact between the heat sinks and the sample. In principle, measurements of the thermal conductivity at different values of clamping pressure are possible, to evaluate the effect of the thermal contact resistance. The pressing system and the support for the sample is a thermal conductance in parallel with the sample, so it has been designed in order to have a low conductance, to minimize the thermal losses from the sample to it. The pressing system consists of two G11 plates separated by 3 small nylon cylinders. The upper plate supports the heater, a copper block with wounded the heating

coil. The junction between the G11 pressing plate and the heater is achieved through a hinge, allowing a maximum angulation of about two degrees, and providing a good contact between the copper and the sample even if the two faces are not perfectly parallel. The lower G11 plate of the pressing system is connected to the upper part of the pressing system with 3 stainless steel rods. The clamping pressure can be varied by acting on the loading springs which compensate also the small differential thermal contraction between the stainless steel rods and the sample holder, so that the compression is almost constant at different temperatures.

All the system is enclosed in a gold plated stainless steel radiative shield, to minimize the radiative losses. Two heaters are placed on the radiative shield in order to get on it a temperature profile similar to that one on the sample. The flange where the radiative shield is attached has the feedthroughs for the thermocouples, the control signals and the heaters and acts as a cold junction for the thermocouples. The thermal sensors are AuFe(0.07% at.w.)-Cromel P thermocouples. This kind of sensors have been chosen for their easy use at low temperatures, small dimensions, low thermal capacity and because of its reliability in vacuum.

The system together with the radiation shield is enclosed in a vacuum chamber (made of stainless steel) which is maintained at a pressure of about 10^{-6} mbar by means of a turbomolecular pump, to avoid convective losses. The vacuum chamber is immersed in the cryogenic fluid. All the dealings of the flanges are indium seals. The maximum dimensions of a sample are **35 mm diameter** and **70 mm length**, and the measuring temperature range is 4.2 – 350 K[12]. Lower temperature measurements, down to 2 K can be available by pumping over the helium bath.

4 HEAT LOSSES IN THE SYSTEM

Many sources of power losses are present in the apparatus: heat conduction through the supporting system, radiation and convection. Each source can cause a wrong thermal evaluation of the power flowing into the sample.

4.1 POWER LOST THROUGH THE SUPPORTING SYSTEM

To evaluate the thermal conductivity we measure the temperature T_1 and T_2, and the power dissipated in the heater. Actually not all the dissipated power flows into the sample. For instance part of the power will flow through the supporting system, which can be considered as a thermal conductance in parallel to the sample. An evaluation of this parasitic conductance is needed to correctly determine the conductance of the sample. In this case the supporting system is described by a sequence of materials thermically connected in series, following the schematization and the model reported in section 2. In this case the model is more accurate because the structure of the supporting system is not so complex as a superconducting coil block, so the calculated conductance is a reliable value.

The temperature profiles along the supporting system calculated with the boundary conditions (temperatures of the heat sinks) $T_1 = 4.2K$, $T_2 = 70K$ and $T_1 = 77K$, $T_2 = 300K$ are shown in fig. 2.

The non smooth temperature profile at the junction point between different materials is a consequence of the heat flow continuity condition, i.e.

$$(\frac{dT}{dx} S\lambda) \mid_{\bar{x}} = (\frac{dT}{dx} S\lambda) \mid_{\bar{x}+\Delta x} \qquad (19)$$

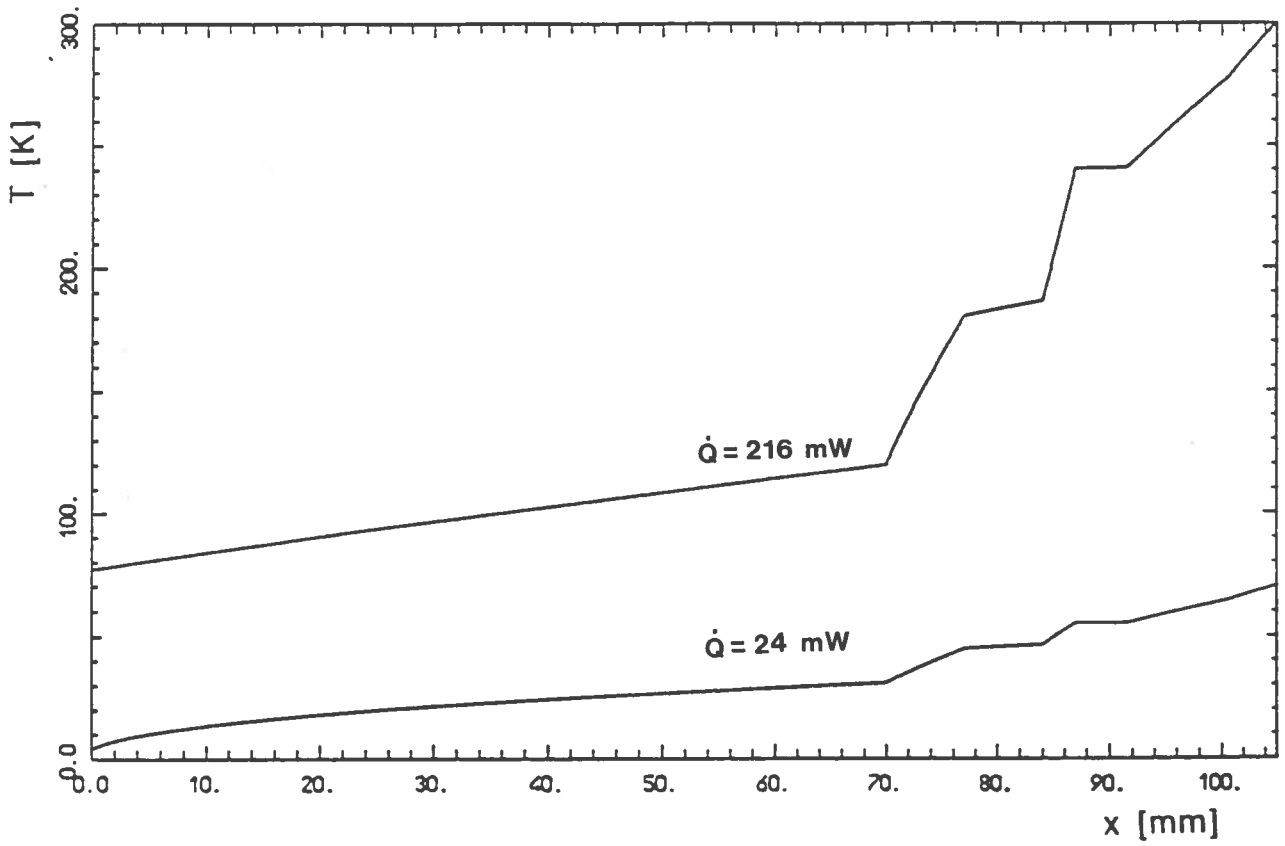

Figure 2: Typical temperature profiles along the supporting system of the thermal conductimeter

The discontinuity of the temperature gradient comes from the sharp variation of S and λ when passing from one material to another. While the change of λ gives actually a discontinuity of the temperature gradient, the discontinuity can be artificially amplified by the rough approximation used for the solution of the equation: the hypothesis that the thermal flow takes place in the whole section of the conductor and the "transition zone" reduces to a point. This is not true because the heat flow lines do not follow the geometrical profile of the conductor but tend to smooth the geometrical discontinuities, so the effective section for conduction is the geometrical one only at a certain distance from the discontinuity.

So the conductance and the power flowing through the system is actually less than the values calculated with the rough model, where the actual section is certainly overestimated.

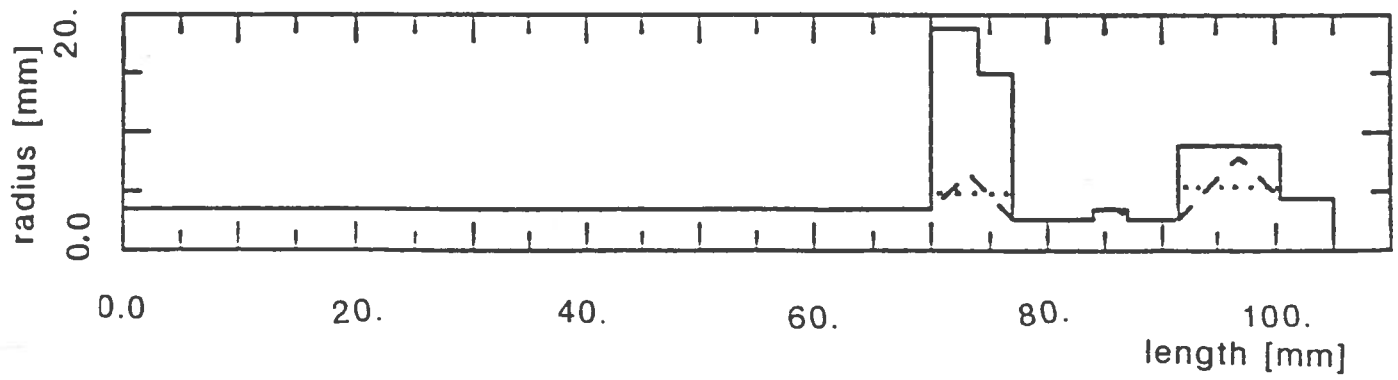

Figure 3: Profile of the supporting system. Solid line: geometrical profile; dashed line: linear smoothing approximation; dotted line: ad hoc approximation

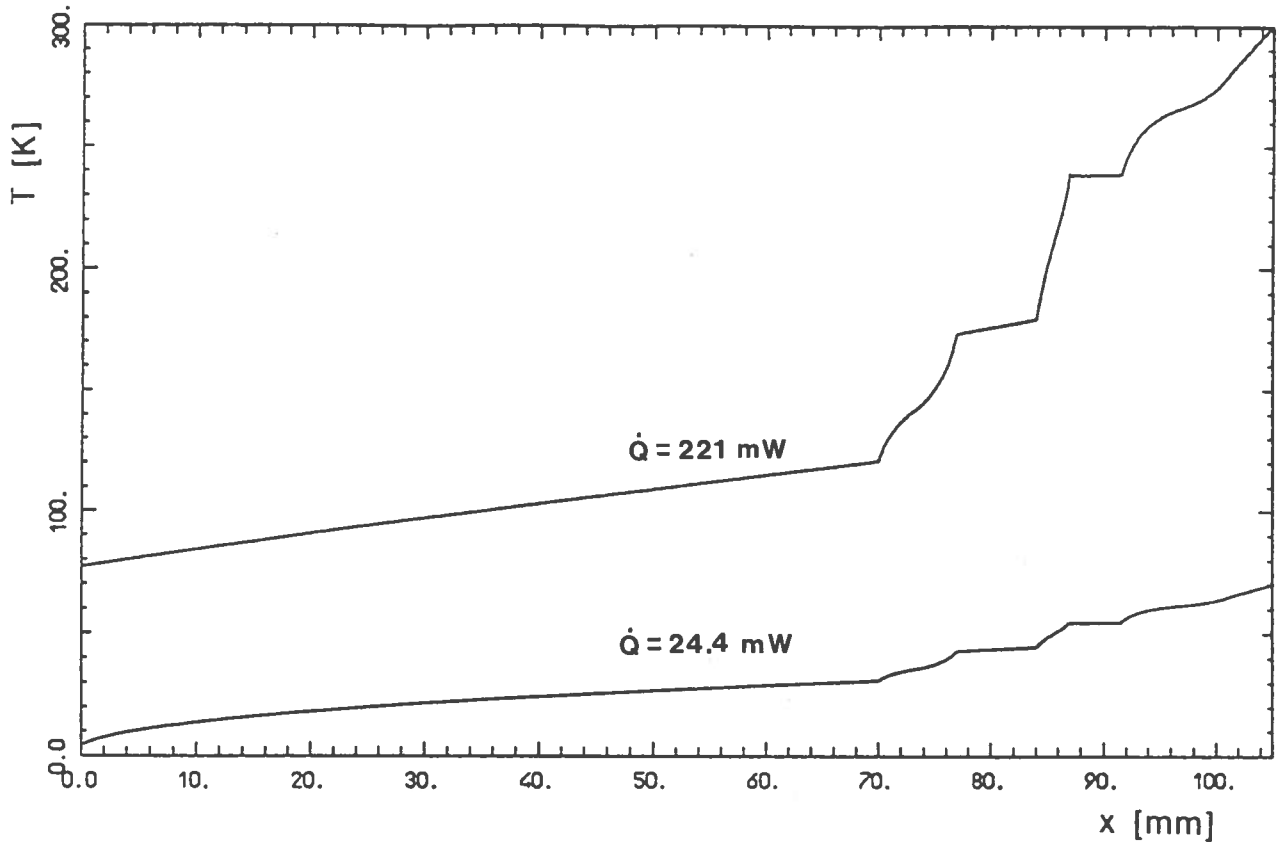

Figure 4: Calculated temperature profile with smoothed sections

By supposing a linear smoothing among the sections as shown in fig. 3 we get the temperature profile shown in fig. 4 and the corresponding power flow is 24.4 mW for $T_1 = 4.2\ K$ and $T_2 = 70\ K$, and 221 mW for $T_1 = 77\ K$ and $T_2 = 300\ K$, (about 38 % less than the non smoothed case).

The linear smoothing overestimates the effect of the transition zone but surely will give estimations closer to the real situation than the "hard edge" approximation. Nevertheless the temperature profiles obtained with the linear smoothing approximation are not much more realistic than the hard edge ones.

A true evaluation of the temperature profile can be achieved by determining the heat flow lines in the transition zone. An approximated ad hoc evaluation of the effective section for conduction gives the temperature profiles of fig. 5 corresponding to different boundary conditions.

Fig. 6 shows the calculated equivalent conductance of the supporting system in ad hoc evaluation model, experimental points are shown too.

4.2 CONVECTIVE LOSSES

A bad vacuum into the conductimeter chamber affects the heat flowing through the sample. According to a simple model, the heat transferred (per unit surface) by conduction through a gas at low pressure P between two surfaces at T_1 and T_2 temperature is given by[13]:

$$\dot{Q} = cost\ \ a_0\ \ P\ \ (T_2 - T_1) \qquad (W/m^2) \tag{20}$$

where:

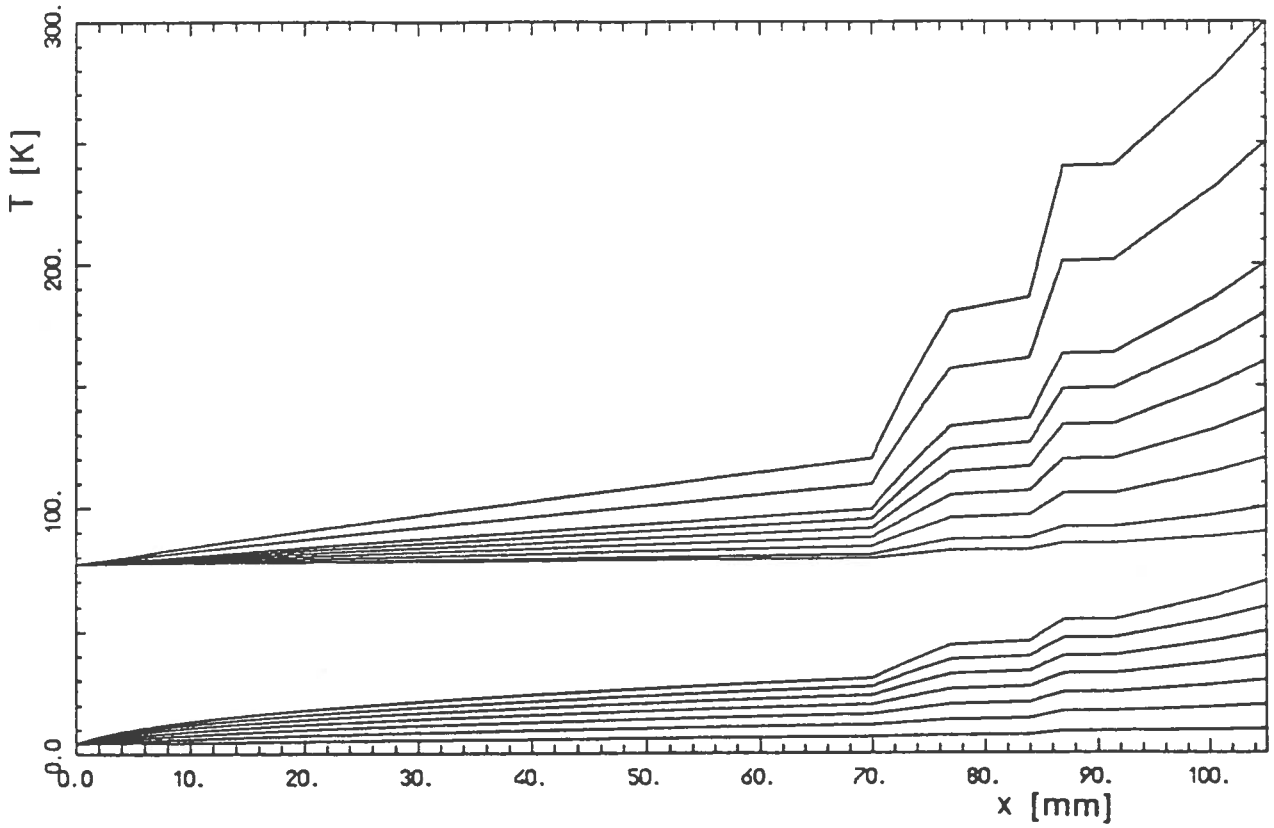

Figure 5: Calculated temperature profiles for different boundary conditions.

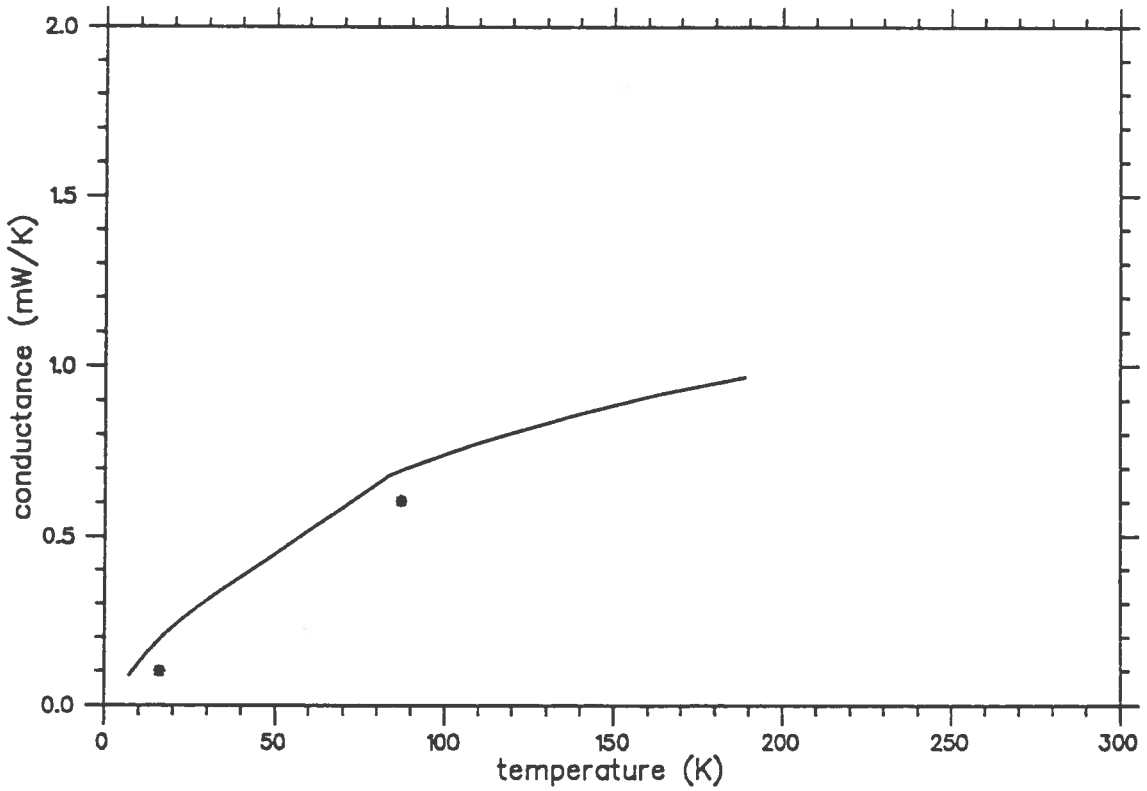

Figure 6: Equivalent conductance of the supporting system of the conductimeter.* Experimental data

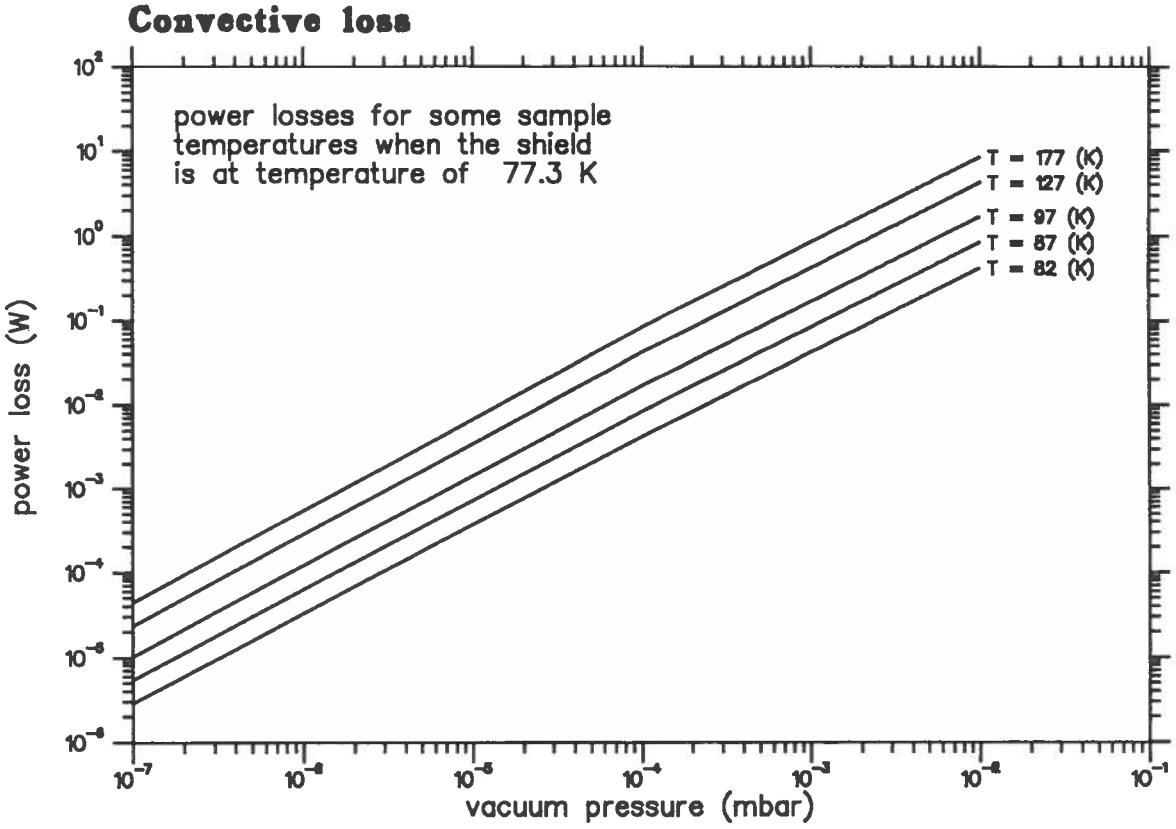

Figure 7: power lost in convection vs. vacuum pressure

$$
\begin{aligned}
cost &= typical\ gas\ constant\ (2.1\ for\ He\ gas) \\
a_0 &= geometric\ factor \\
P &= gas\ pressure
\end{aligned}
$$

This formula describes the heat transfer for low pressure gases, when the mean free-path l of a molecule is much greater than the dimension of the vacuum chamber d (e.g. $l \gg d$), and the value of 2.1 for the constant is the He typical value. Given a geometric factor as $a_0 = 0.36$ [13] (for our sample typical dimension), we obtain the heat transfer vs. gas pressure, see figure 7.

In figure 8, the power loss for different level of vacuum versus the sample mean temperature in the two cases for shield temperature of 4.2 K (for He) and 77.3 K (for N) is plotted. As shown, at 10^{-5} $mbar$ these kind of loss can be neglected.

4.3 RADIATIVE LOSSES

There are many and different models describing radiative heat transfer between two surfaces at different temperature[14], related by the Stefan-Boltzmann constant and four-power of the temperature. Because of the T^4 behaviour, radiation losses usually are negligible below 20 K but can became very important when T is the temperature of the liquid nitrogen. To evaluate the losses three models were chosen to describe radiative heat exchange between two surfaces: in every one the first surface completely includes the second one. All these models give the heat radiated between two surfaces depending on the surfaces form: in the

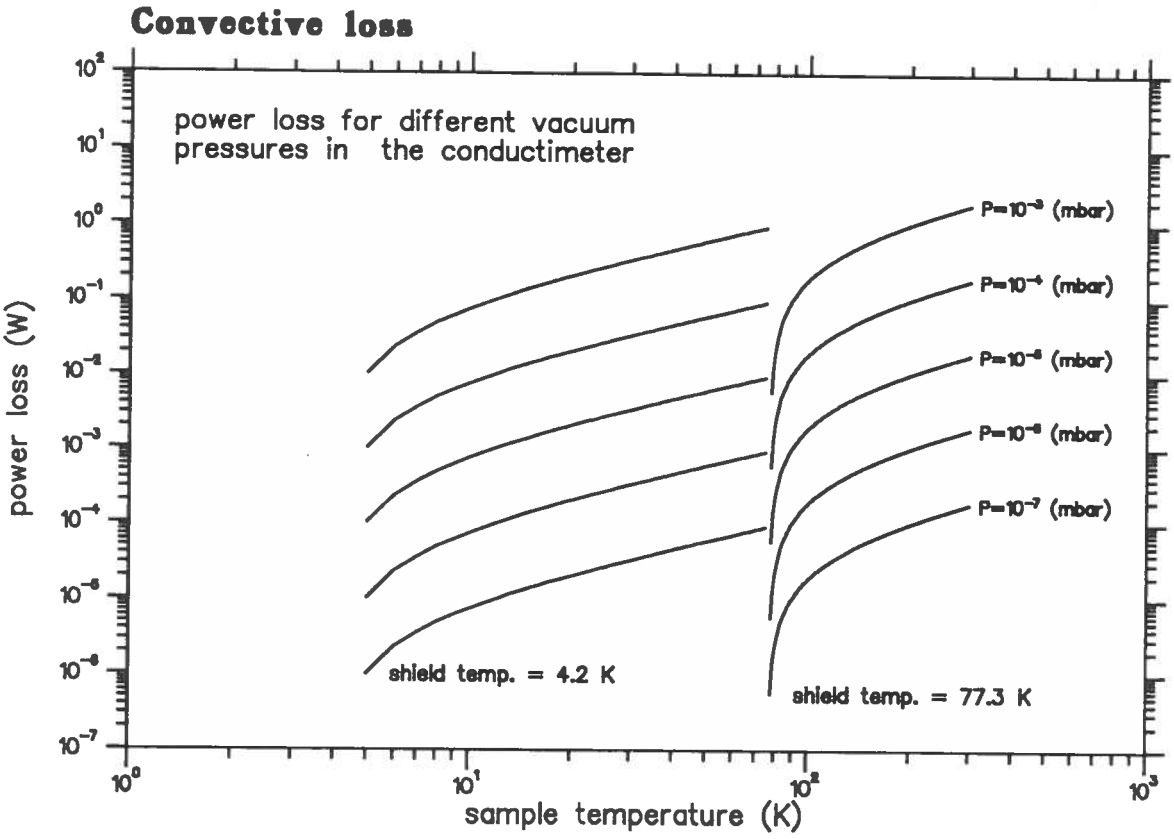

Figure 8: power lost in convection vs. sample temperature

first model the sample and the thermal shield are two generic shape surfaces, the greater (thermal shield) including completely the smaller (sample). In this model, the simplest one, the heat radiated by the S surface at T_1 temperature toward the other surface at T_2 temperature is given by:

$$\dot{Q} = S\ \varepsilon\ \sigma\ (T_2^4 - T_1^4) \qquad (W) \tag{21}$$

where:

$$\begin{aligned} \varepsilon &= \textit{inner surface emissivity} \\ \sigma &= 5.67 \times 10^{-8}\ (W/m^2K^4)\ \textit{Stefan} - \textit{Boltzmann constant} \end{aligned}$$

In the other two models the emissivity of both the surface and a geometric factor appear. In one case the thermal shield and the sample are described as two concentric cylinders; in the other case they are described as two concentric spheres. The thermal flow by one surface (sample) toward the second one (thermal shield) is:

$$\dot{Q} = S\ \varepsilon_1\varepsilon_2\ F_{1,2}\ \sigma\ (T_2^4 - T_1^4) \qquad (W) \tag{22}$$

where:

$$\begin{aligned} \varepsilon_1 &= \textit{first surface emissivity} \\ \varepsilon_1 &= \textit{second surface emissivity} \\ S &= \textit{sample surface} \\ F_{1,2} &= \textit{exchange factor} \end{aligned}$$

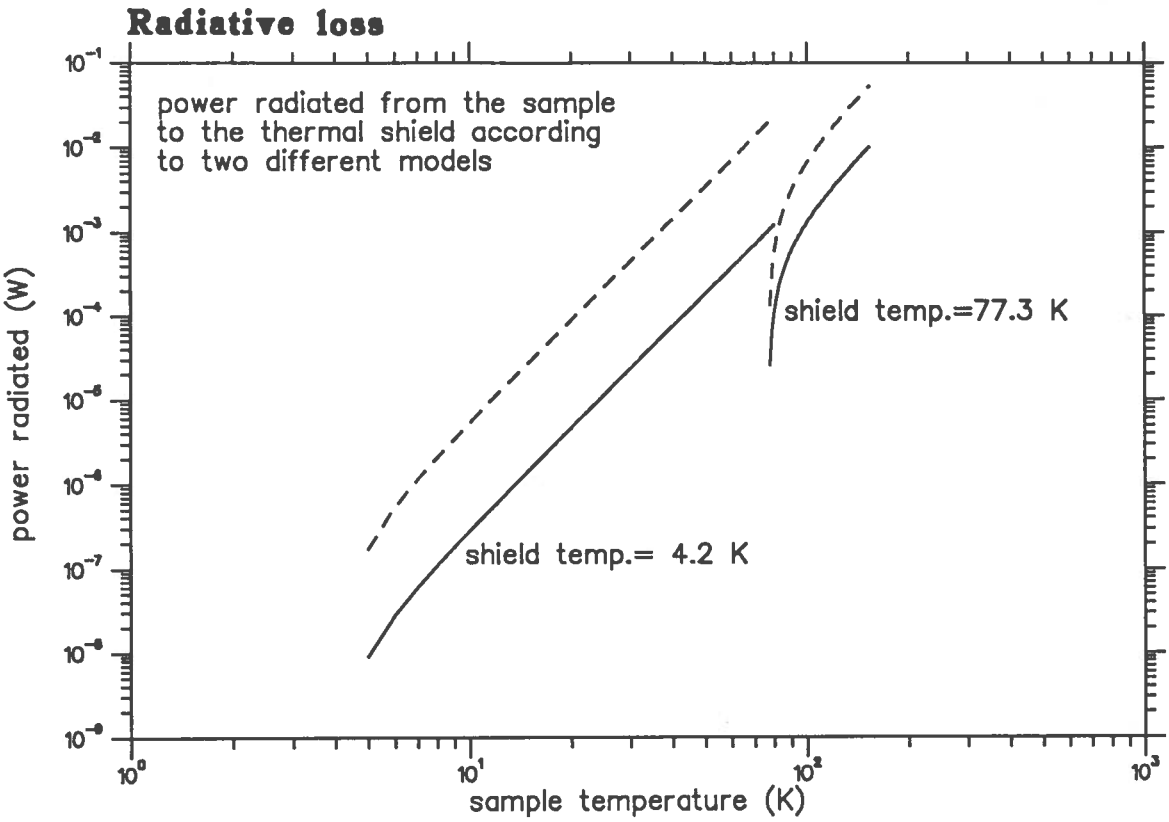

Figure 9: power radiated by the sample to the shield

The exchange factor $F_{1,2}$ depends on the symmetry chosen, cylindric or spheric (for example, $F_{1,2} = 0.35$ for the cylindric symmetry for our sample typical dimension). In figure 9 two models are presented: the power radiated is plotted vs. sample temperature, being thermal shield temperature held at 4.2 K (for liquid helium) and at 77.3 K (for liquid nitrogen). In this figure we suppose $\varepsilon_1 = 0.3$ for the sample (for both the models) and $\varepsilon_2 = 0.03$ for the thermal shield, having a gold surface.

In figure 9 dashed line curve describes equation 21, full line equation 22 and it is reported for the cylindric symmetry only, because the spheric symmetry gives an almost identical result. As shown, the two equations give results which differ by an order of magnitude, and we usually use the cylindric model, which appears more realistic. According to this model, we can say that when the temperature difference between the sample and the thermal shield is not greater than $20 \div 30$ K, the radiated power is about 10^2 times less than the total supplied power.

In fact, if we consider for example the power radiated by the Nb_3Sn sample (described in the next section) at $T = 30$ K toward the thermal shield at $T = 4.2$ K, it is about $\dot{Q} \simeq 10^{-4}$ (W), while the power given to the sample by the warm heater is, in this case, $\dot{Q} = 0.17$ (W). When the sample is at $T = 100$ K and the shield at $T = 77.3$ K, the power radiated is about $\dot{Q} \simeq 10^{-3}$ (W) and heat generated in the resistance is $\dot{Q} = 0.72$ (W). In these cases, radiative losses can be neglected.

Anyway in case of measurements with high ΔT are needed, the shield is provided with two heaters and two thermocouples to generate along the shield almost the same thermal gradient that exists along the sample. The shield, in order to be mechanically strong, is made of stainless steel, 0.2 mm thick, and it has a large conductance: for example, at $T = 80$ K

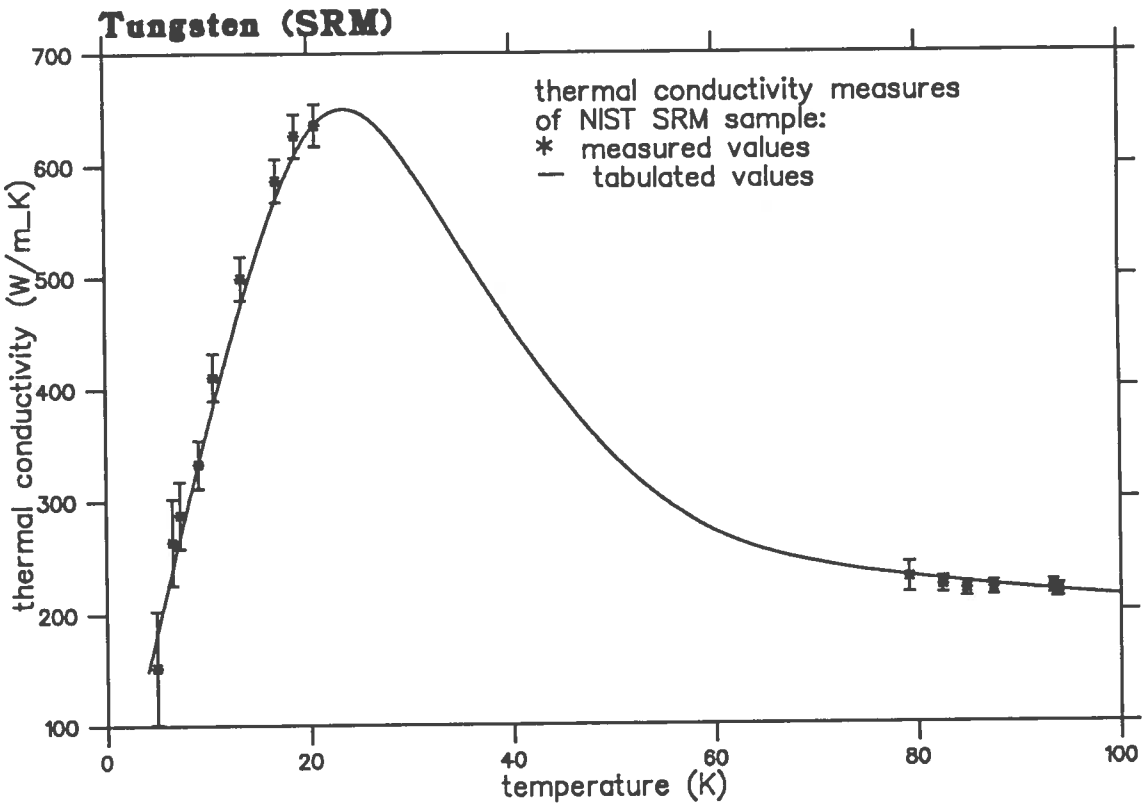

Figure 10: tungsten thermal conductivity

it is about $4.4 \times 10^{-3}\ W/K$, between the bottom heater and the top flange.

If the Nb_3Sn sample is heated up to a mean temperature of 100 K, there is a temperature difference of about 35 K between the heat sinks. To reach the same thermal gradient, about 0.14 W must be generate in the shield, but this heat power can warm the thermal anchorage of the thermocouples (which is the mechanic anchorage of the shield) and modify the temperature measurements. So it is better to generate in the shield a thermal gradient smaller than in the sample to avoid this kind of problem.

Indeed, this effect is greater in liquid helium measurements, because of the conductance of the shield and of the thermal anchorage is smaller again, but in this temperature range we are not forced to use it.

5 APPARATUS CALIBRATION

Calibration of the conductimeter was achieved by measuring reference materials of known λ. A *tungsten NIST SRM (Standard Reference material)* sample is used (3.2 mm diameter, 50 mm length) with 3 temperature sensors along the sample ($AuFe/KP$ thermocouples). A good thermal contact between thermocouples and the sample was achieved by 3 copper rings, in contact with the sample, in which the temperature sensors are fixed.

After first measurements and minor modification in the path of the wires (both thermocouples and heater) to avoid risk of thermal short circuit, we got a good agreement between our measurements and $NIST$ reference values, see figure 10.

We are confident that our absolute accuracy is within 10 % with one limitation: the

temperature difference in the sample must be at least 1 K and the power flow should not be larger than 750 mW, limiting the maximum achievable ΔT. The reasons of these limitations, which are important for temperature $T < 6\ K$ and $T > 30\ K$ can be understood after a brief analysis of the error sources.

5.1 ERROR SOURCES

Experimental thermal conductivity values are obtained through measurements of many quantities: $\dot{Q}$, ΔT, S and L. Using the general formula error propagation and indicating with σ the standard deviation (or the uncertainty) we obtain 3:

$$\frac{\sigma_\lambda}{\lambda} = \sqrt{\left(\frac{\sigma_{\dot{Q}}}{\dot{Q}}\right)^2 + \left(\frac{\sigma_L}{L}\right)^2 + \left(\frac{\sigma_S}{S}\right)^2 + \left(\frac{\sigma_{\Delta T}}{\Delta T}\right)^2} \tag{23}$$

In many measurements the temperature is the dominant error source, since instrument sensitivity is 0.1 degree and for small heat powers the measured ΔT can be less than 0.5 degree. In this case:

$$\frac{\sigma_{\Delta T}}{\Delta T} \gg \frac{\sigma_{\dot{Q}}}{\dot{Q}}\ ;\ \frac{\sigma_S}{S}\ ;\ \frac{\sigma_L}{L}$$

and we can reduce the expression 23 to:

$$\frac{\sigma_\lambda}{\lambda} \simeq \frac{1}{\Delta T}\sqrt{(\sigma_{T_1})^2 + (\sigma_{T_2})^2} \tag{24}$$

because in the determination of the ΔT errors we have to take in account the overlapping of the errors on the measurement of the two temperatures (T_1 and T_2).

5.2 ERROR ANALYSIS AND ACCURACY ESTIMATION

In thermal conductivity calculation by mean of:

$$\lambda = -\frac{\dot{Q}\ L}{S\ \Delta T}$$

a correct evaluation of $\dot{Q}$, i.e. the heat flow corresponding the ΔT, is of primary importance.

The first remark must be done about the current leads. The warm heater was made with a *manganine* wire, with a resistance of 25.7 Ω/m: so part of the power generated by the wire was not given to the warm heater but it was lost toward the upper flange of the condutctimeter (see fig. 1); it was about 2% of the entire heat power given to the measuring sample.

On the other hand, it can not be substitute by a wire with a too small resistance, like one made of copper, because if ρ is very small, then λ is very great: in this case the wire can conduct a considerable part of the power generated toward the upper flange. A copper wire with a diameter of 0.1 mm can conducts away about 2% of the whole generated heat.

The best solution is then to use a cryogenic wire of a copper alloy to realize the current lead. We choose the QUAD-LEAD^{TM} (from LakeShore Cryotonics, Inc., a quadrupole wire of phosphor bronze, $\phi = 0.2\ mm$). Its electrical resistance is 2.85 Ω/m and its thermal

conductivity is about 10^3 times less than copper conductivity. The power losses through this wire is less than 0.3% of the whole generated power.

Other sources of thermal losses are present, like parasitic thermal conductance caused by the thermocouples wires or by the compressing system.

The thermal conductance of the compressing system is about 0.2% at 20 K up to 2% at 100 K of the SRM tungsten thermal conductance, while the thermal conductance of the thermocouple wires is about 0.3% at 20 K up to 0.6% at 100 K of that of the same sample. This comparison shows that the presence of the compressing system and of the thermocouple wires can not be neglected.

The whole parasitic thermal conductance can so be estimated around 2% of that of the SRM tungsten bar and then we suppose that a part of the heat flowing into the sample is taken away through the stainless steel rods and through the thermocouple wires. Calling $\dot{Q}_{loss}$ this part of the power generated by the heater but lost through the compressing system and the thermocouples, we can write:

$$\dot{Q}_{tot} = \dot{Q}_{eff} + \dot{Q}_{loss}$$

where $\dot{Q}_{tot}$ is the whole generated power and $\dot{Q}_{eff}$ is the part of it really flowing into the sample.

If $\dot{Q}_{tot}$ is used instead of $\dot{Q}_{eff}$ an over-estimation of λ occurs: in fact the ΔT measured is corresponding to $\dot{Q}_{eff}$ and we can think it is less than the ΔT that the whole $\dot{Q}_{tot}$ could generate. As said before, the whole conductivity of the compressing system and of the thermocouples wires is about 1.5% of the *tungsten SRM* conductivity and so about the 1.5% of the power generated by the heater is lost through them. If the radiative and the convective heat losses and conduction through the power leads are considered too, it can be come to the conclusion that the λ experimental values are greater than the actual one by about 3%.

A strict analysis of the *tungsten SRM* thermal conductivity measurements shows this problem (see fig. 10). The measured values in the coldest range (under 10 degree) can not be considered because, as previously said, the error on λ measurements is as greater as smaller is ΔT, and in these cases the error on ΔT is so great to hide the error on $\dot{Q}$. But for the λ values between 10 and 30 K it can be seen that they exceed tabled values of about $2 \div 3\%$, confirming the previous analysis.

As previously said, it is important to consider the ratio of thermocouple conductance versus sample conductance (and compressing system conductance versus sample one). When we consider the other thermal conductivity measurements made on coil block data, presented in the next section, we get an over evaluation of the real values that can be estimated around 5% for $NbTi$ and Nb_3Sn . In fact, for example, the thermal conductance of the compressing system at $T = 50\ K$ is about $C_{comp.sys.} = 0.45 \times 10^{-3}\ (W/K)$, while, as it will be shown, the Nb_3Sn sample conductance is about $C_{Nb_3Sn} = 14 \times 10^{-3}\ (W/K)$ at $T = 50\ K$: this means that $C_{comp.sys.}$ is about 3.5% of the C_{Nb_3Sn}. Now it can be said that to have good enough measurements between 4 K and 20 K temperature, it is necessary that the sample conductance is:

$$5 \times 10^{-3} < C < 20 \times 10^{-3} \quad (W/K)$$

In fact, to have thermal gradients not smaller than 0.5 K (that is, an error on the thermal conductivity measurement not greater than 10%) with small heat supplied too (and then at low temperatures), it must be: $C < 20 \times 10^{-3}\ \ W/K$. On the other hand, to have a

compressing system and thermocouple wires conductance not greater than 5% of the sample conductance (into $4 \div 20K$ range) it must be : $C > 5 \times 10^{-3}\ W/K$. Moreover, if C is very small in the sample there will be a great thermal gradient and because just the same thermal gradient will must be generated in the shield, causing the troubles previously shown. Now we could notice that, according to the former remarks, it is necessary to complete the error analysis: into equation 23 it can not be neglected the error on the heat flow at least when the temperature difference is greater then 1 K:

$$\frac{\sigma_\lambda}{\lambda} \simeq \sqrt{\left(\frac{\sigma_{\Delta T}}{\Delta T}\right)^2 + \left(\frac{\sigma_{\dot{Q}}}{\dot{Q}}\right)^2}$$

Since:

$$\lambda\ \frac{\sigma_{\dot{Q}}}{\dot{Q}} \simeq\ \lambda \frac{C_{comp.sys.}}{C} = C_{comp.sys.}\ \frac{L}{S}$$

where:

$$\begin{array}{lcl} C_{comp.sys.} & = & compressing\ system\ conductance \\ C & = & sample\ conductance \\ S & = & sample\ section \\ L & = & sample\ length \end{array}$$

a very useful formulation of the errors is given by:

$$\frac{\sigma_\lambda}{\lambda} = \sqrt{\frac{(\sigma_{T_1})^2 + (\sigma_{T_2})^2}{(\Delta T)^2} + \left(\frac{C_{comp.sys.}\ L/S}{\lambda}\right)^2} \tag{25}$$

6 MEASUREMENTS ON COIL BLOCKS

Some measurements were made on coil blocks cut from real coils, made by $NbTi$ and Nb_3Sn, wound with rectangular and round section cables. In all these cases transverse thermal conductivity was measured, because it is of great interest in magnet protection, as previously said.

To measure a sample it is necessary to fit it to the conductimeter, so its dimension must not exceed the maximum one permitted by the system and the sample faces which are in direct contact with the heat sink must be as smooth as possible to allow a good thermal contact. Usually the thermal contact is improved by means of a special cryogenic grease, containing a high percentage of copper. But first of all the sample must be prepared to make its conductance inside the optimum conductimeter working range, as previously described. Sometimes, this fact forces us to measure the sample more than once, to obtain data with errors as low as possible.

Measured data are compared with conductivity curves calculated from thermal conductivities of they components: figure 11 is a plot of the measurements of the transverse thermal conductivity of a Nb_3Sn/Cu coil wound with a flat cable into the temperature range between $4 \div 150\ \ K$; figure 12 shows the measurements of the thermal transverse conductivity of a small $NbTi/Cu$ coil wound with a round wire into a low temperature range ($4 \div 40\ \ K$), which is the most interesting one for our purposes. Measurements were repeated on both the coil blocks and a good repeatability of the data was obtained, as shown in figures.

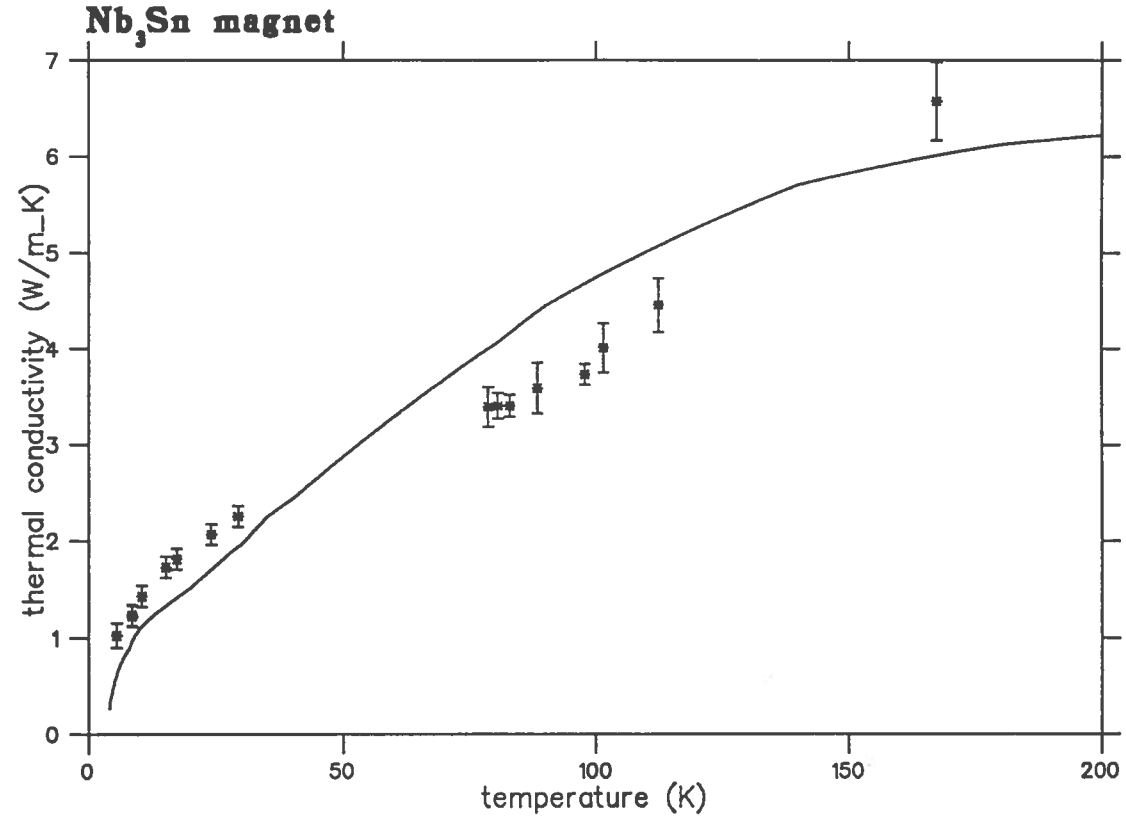

Figure 11: transverse thermal conductivity of a Nb_3Sn coil

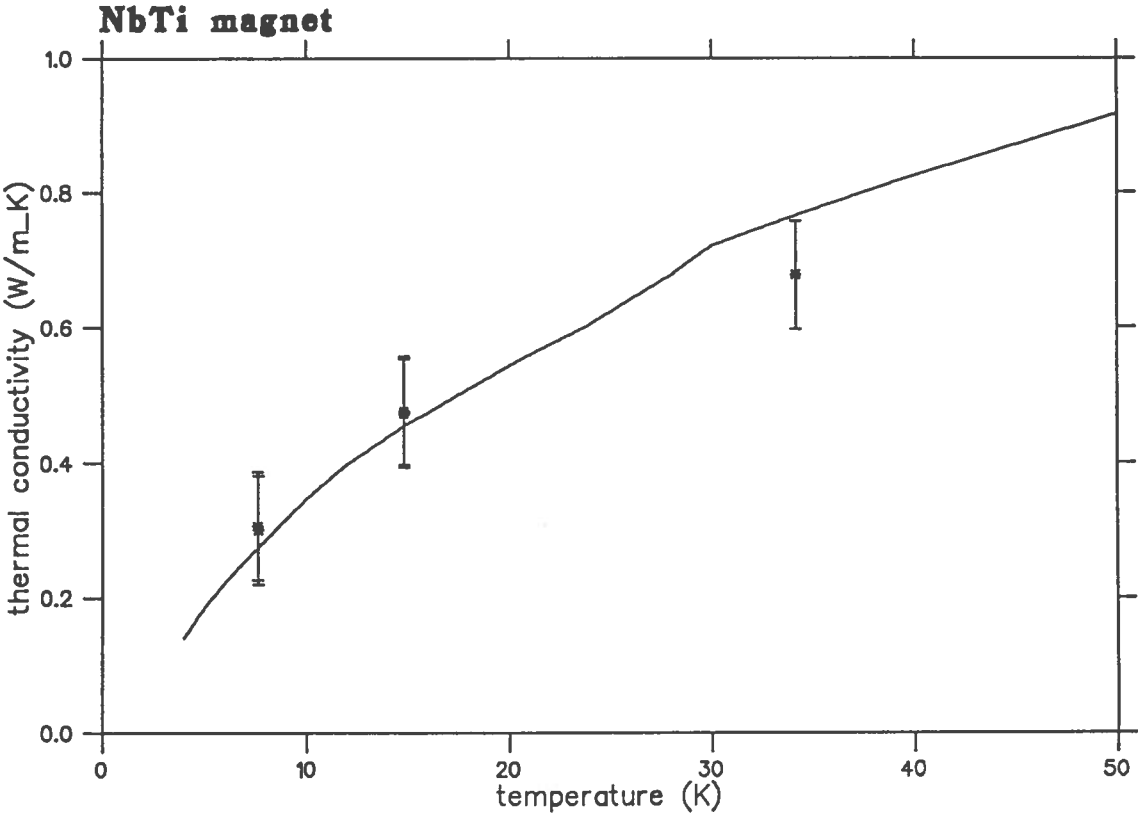

Figure 12: transverse thermal conductivity of a $NbTi$ coil

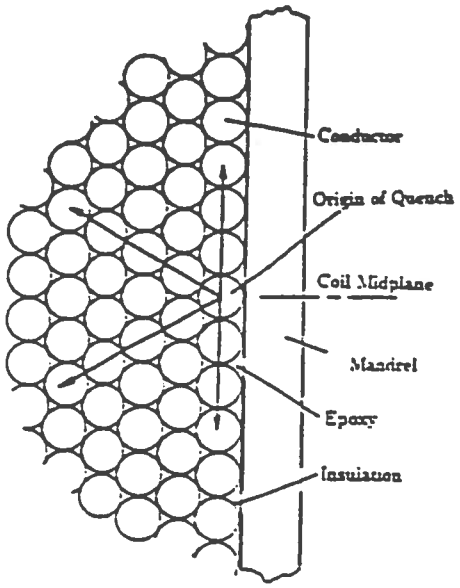

Figure 13: round–wire coil section

Calculated curves are obtained using suitable routines for thermal properties evaluation. By these routines, thermal conductivity of a composite like a coil block can be calculated like a thermal circuit, where the thermal conductances are connected either in series or in parallel. In this schematization the thermal conductivity of each element must be known, which requires to know both the $\lambda = \lambda(T)$ of each material and the temperature of the element. By assuming a fixed temperature value is then possible to evaluate the effective conductance following the same rule for electric circuit. We refer to this schematization for composite as to "lumped circuit" approximation.

We made distinction between rectangular and round cable. In fact, in each case, a different arrangement of the materials composing the coil is obtained. The routines for thermal conductance evaluation were built for rectangular cables only, but they can work well enough with round cables too. In figure 13 is shown a typical round-wire coil package.

A library of material properties enable us to calculate many different kinds of composite cables into the temperature range between 4 and 300 K.

The richest section of the library is that relative to the thermal conductivity data: it is possible to refer to any superconducting materials, like $NbTi$, Nb_3Sn , V_3Ga , Nb, Va, Pb, Ti; or to stabilizing metals like Al, Cu, $CuSn$, Ta, $BeCu$; or to some insulator like *vitreous silica*, *silica glass*, *Teflon*, $G10$ and $G11$ in normal and parallel direction, *Nylon*, *Perspex* and $G10$ rod; or to other metals largely used in magnet facility, like *stainless steel*, *Phosphorous Deoxidate Copper* or reference material like W.

Then, starting from the thermal property of each single material it is possible to calculate longitudinal and transverse thermal conductivity of a composed cable. As shown in figures 11 12, routines to calculate thermal conductivity of a composed cable give a good agreement with the experimental data, in spite of the strong anisotropy and the non homogeneity of a coil.

Our purpose is to increase the number of these routines and of this library, because

a correct description of the transverse thermal conductivity of a coil is one of the most important aspect in magnet design and protection.

Finally two photographs of the thermal conductivity apparatus are shown: in figure 14 the sample holder and in figure 15 the thermal shield and the vacuum chamber.

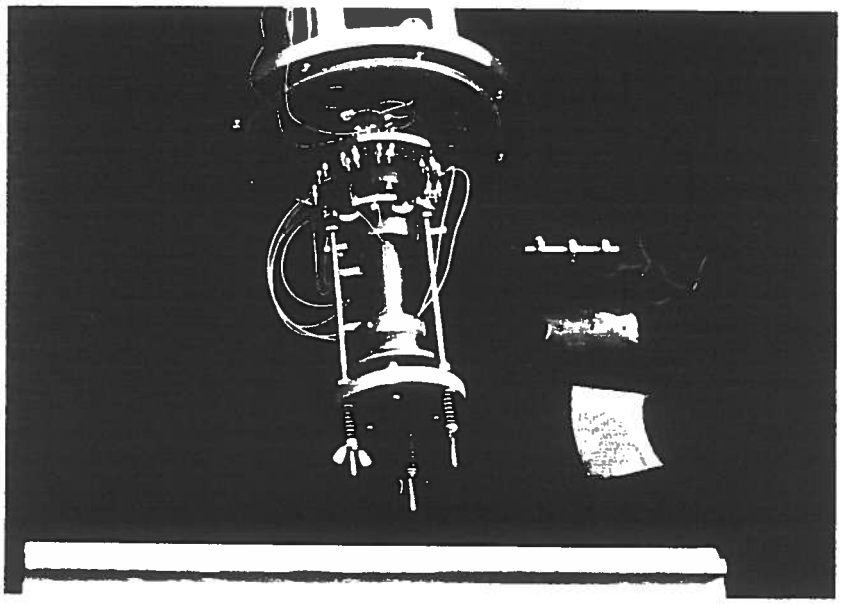

Figure 14: photograph of the sample holder without thermal shield and vacuum chamber

Figure 15: photograph of the thermal shield of the apparatus and the vacuum chamber

Acknowledgements

The authors are indebted with Dr. C. Barrilá who did the first design of the apparatus and with Mr. A. Leone and Mr. D. Pedrini for their help in vacuum and cryogenic operations.

References

[1] E. Acerbi, F. Alessandria, G. Baccaglioni, C. Birattari, E. Fabrici, L. Rossi, A. Sussetto, "High field superconducting solenoid for the LASA in Milan," *IEEE Trans. on Mag.* , Vol.24, No.2, March 1988, pp. 1417-1420.

[2] J.E.C. Williams, S. Pourrahimi, Y. Iwasa, L. J. Neuringer, "600 MHz spectrometer magnet," *IEEE Trans. on Mag.*, , Vol.25, No.2, March 1989, pp.1767-1770.

[3] P. Turowski, Th. Schneider, "19.3 T with a superconducting magnet," *IEEE Trans. on Mag.,* Vol.24, No.2, March 1988, pp.1063-1066.

[4] A. Ishiyama and Y. Iwasa, " Quench propagation velocity in an epoxy-impregnated Nb_3Sn superconducting winding model," *IEEE Trans. on Mag.,* Vol. 24, No.2, March 1988, pp. 1194-1196

[5] C.H. Joshi and Y. Iwasa, "Prediction of current decay and terminal voltages in adiabatic superconducting magnets," *Cryogenics,* 1989 Vol.29 March, pp.157-167.

[6] E. Acerbi, G. Baccaglioni, M. Canali and L. Rossi, "Experimental study of the quench properties of epoxy impregnated coupled coils wound with NbTi and Nb_3Sn ", *IEEE Trans. on Mag.,* Vol. 28, No.1, january 1992, pp. 731.

[7] M.N. Wilson, *Superconducting Magnets,* Clarendon Press Oxford 1983, p. 208

[8] R.P. Reed and A.F. Clark, *Materials at low temperatures,* American Society for Metals, 1983, pp.133-161.

[9] J.E. Jensen, R.B. Steward, W.A. Tuttle, *Selected Cryogenic Data,* Bubble Chamber Group of Brookhaven Nat. Lab., Nov. 1966, section VII.

[10] J. G. Hust, A. B. Lankford, "International Journal of thermophysic", Vol.3, No.1, 67-77.

[11] J.C. Hust, P.J. Giarratano, "Thermal conductivity" in *Semi - annual Technical Report on Material Research in Support of Superconducting Machinery,*NBSIR 74-359,1974a,Nat. Bureau of Standards, pp. 29-44.

[12] C.Barrila', F. Broggi, L.Rossi, G.Volpini, "Measurements of Thermal Conductivity of Epoxy Impregnated $NbTi$ and Nb_3Sn Windings", *IEEE Trans. on Mag.,* Vol.28, No.1, January 1992, pp.900-903.

[13] Guy K. White, "Experimental techniques in low-temperatures physics", Claredon Press Oxford 1987, pp. 127-131.

[14] R. Siegel, J. R. Howell, "Thermal radiation heat transfer", International Student Edition, McGraw Hill Kogakusha 1972, p. 243 and p. 787.

a correct description of the transverse thermal conductivity of a coil is one of the most important aspect in magnet design and protection.

Finally two photographs of the thermal conductivity apparatus are shown: in figure 14 the sample holder and in figure 15 the thermal shield and the vacuum chamber.

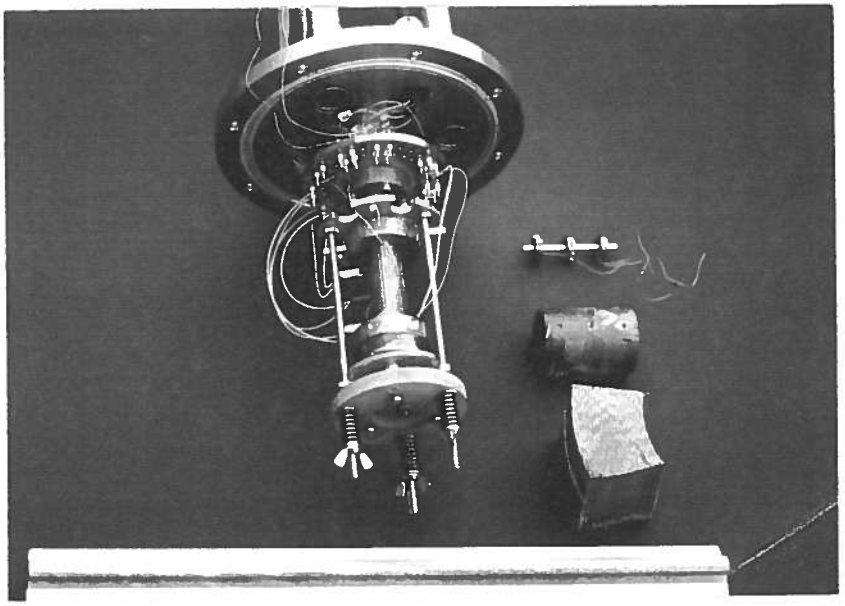

Figure 14: photograph of the sample holder without thermal shield and vacuum chamber

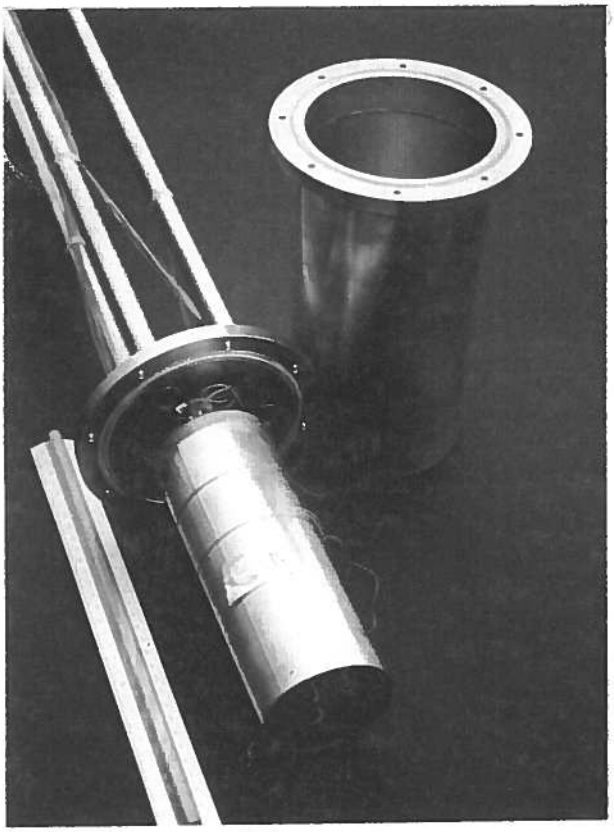

Figure 15: photograph of the thermal shield of the apparatus and the vacuum chamber